An investigation on methods for axis detection of high-density generic axially symmetric mechanical surfaces for automatic geometric inspection

Guardiani E.[1] and Morabito A.[2]

[1] Department of Industrial Engineering, University of L'Aquila, L'Aquila, Italy
[2] Department of Engineering Innovation, University of Salento, Lecce, Italy

Abstract.
The detection of the symmetry axis from discrete axially symmetric surfaces is an interesting topic, which is transversal to various fields: from geometric inspection to reverse engineering, archeology, etc. In the literature, several approaches have been proposed for estimating the axis from high-density triangular models of surfaces acquired by 3D scanning. The axis evaluation from discrete models is, in fact, a very complex task to accomplish, due to several factors that inevitably influence the quality of the estimation and the accuracy of the measurements and evaluations depending on it. The underlying principle of each one of these approaches takes advantage of a specific property of axially symmetric surfaces. No investigations, however, have been carried out so far in order to support in the selection of the most suitable algorithms for applications aimed at automatic geometric inspection. In this regard, ISO standards currently do not provide indications on how to perform the axis detection in the case of generic axially symmetric surfaces, limiting themselves to addressing the issue only in the case of cylindrical or conical surfaces. This paper first provides an overview of the approaches that can be used for geometric inspection purposes; then, it applies them to various case studies involving one or more generic axially symmetric surfaces, functionally important and for which the axis must be detected since necessary for geometric inspection. The aim is to compare, therefore, the performances of the various methodologies by trying to highlight the circumstances in which these ones may fail. Since this investigation requires a reference (i.e. the knowledge of the true axis), the methodologies have been applied to discrete models suitably extracted from CAD surfaces.

Keywords: Axis of symmetry, Geometric Inspection, Axially Symmetric Surfaces, High-density triangular models, Geometrical Dimensioning and Tolerancing.

1. INTRODUCTION

In mechanical field, axially symmetrical surfaces are of particular interest for the functional role they perform in numerous mechanical components. Geometric inspection frequently requires the axis detection from these surfaces to verify the product conformity to geometric specifications given for controlling certain geometrical or dimensional properties, referred to as characteristics [1]. In the Geometric Product Specification (GPS) language, the axis of an ideal axially symmetrical surface is commonly used also as datum [1]. In all these cases, the quality of the axis detection can significantly influence the reliability of the geometrical verification result, so that the accuracy of this evaluation is to be considered a critical factor for geometric inspection of axially symmetric surfaces.
The need to evaluate the axis is, additionally, required in all those specific application contexts where a high-level analysis of the component geometry is to be performed in order to detect some geometric properties of particular interest for their semantic role, such as in the reverse engineering [2]. Automatic geometric inspection, which is currently attracting much interest due to the latest developments in 3D digitalization, also looks with interest at algorithms for estimating the axis of axially symmetric surfaces.
Laser scanners, nowadays, allow extracting high-density point clouds in a very short time (over 30000 points per second) and with increasingly high accuracy. This has opened the way to new methodologies able to recognize automatically several types of features, through the investigation on the recurrence of differential geometric properties (such as normal, principal curvatures, etc.), and to virtually simulate even complex 3D analytical references. Thanks to these methodologies, the geometric verification can be performed automatically without the need for a CAD model, neither for partitioning the discrete model nor as reference for the error evaluation [3]. An overview of these methodologies has been recently proposed in [4].
High-density digitalization of surfaces is opening up new opportunities, such as:
-) the *definition of novel geometric properties to inspect*, such as the new form errors proposed to verify characteristics not yet considered by current GPS standards [2-3].
-) the *development of new procedures for a more robust verification process of traditional tolerances*, such as the evaluation of the generatrix straightness error [2-3].

-) the *definition of automatic methodologies for the segmentation of discrete geometric models able to differentiate the surface features for functional importance*. In this respect, a methodology based on fuzzy logic has been recently proposed for distinguishing primary features from the secondary ones (such as fillets, rounds and grooves), in agreement with what is done in the engineering practice [5, 6]. In the perspective of an automatic geometric verification, this is important since the secondary features are not subject to explicit geometric specifications, but to general tolerances according to ISO 2768 [7].

The axis is defined by ISO-GPS standards as a symmetry feature [8]; as it is the situation feature for axially symmetric surfaces, its evaluation is necessary to orient and to locate any surface of this geometric type [9]. In particular, the axis of symmetry is not an integral feature so that it does not exist physically. This implies that it is a feature that is not found on the acquired surface, but it has to be derived from the points extracted during the measurement of the object [10].

For discrete models, obtained in the form of high-density point clouds or triangular meshes by 3D scanning, the axis evaluation is a very complex task to accomplish due to several reasons. Firstly, any discrete model can only provide an approximate representation of the original smooth surface of the object. Because the surface of this model is not fully differentiable, the differential geometric properties, often required for the axis evaluation (such as normals and curvatures), must be recognized and cannot be directly evaluated [2-3]. In addition, the points of a discrete model extracted from the surface during 3D scanning never lie on an ideal axially symmetric geometry. Generally, they are affected by unavoidable measurement and manufacturing errors so that the cross sections of these surfaces, for example, are neither circular nor coaxial with each other [3]. These factors inevitably influence the quality of the axis detection and consequently the accuracy of the measurements and evaluations depending on it.

ISO standards address the problem of the axis detection only in the case of cylinders and cones. The axis, in particular, is estimated as the situation feature of an ideal cylinder (or cone) approximating the real sampled cylindrical (or conical) surface based on a given association criterion. The standard ISO 1101 specifies several criteria, such as Minimax (or Chebyshev), Gaussian, Minimum Circumscribed and Maximum Inscribed. Three different options are, additionally, available for Chebyshev and Gaussian criteria: with material external or internal constraint and without constraint [1]. The axis estimated by association may sometimes be subjected directly to a geometric verification of orientation or localization. More often, it is deployed to evaluate other geometric errors, such as those of roundness or axis straightness. In these cases, for example, the axis identifies the perpendicular planes (referred to as *primary enabling features* [8]) required to extract the integral section lines (approximately circular) by the transverse cut of the measured surface. In the specific case of axis straightness error, the feature subjected to the geometric verification is the *derived median line* defined as the set of centers of the 2D circles associated, based on an assigned criterion, with the integral circular lines previously extracted.

At present, ISO-GPS standards provide no further indications on how to perform these tasks when the axially symmetric surface is not referable to cones or cylinders. These surfaces, referred to here as generic axisymmetric, include both those ones deriving from the revolution around an axis of an analytical curve (for example the circular arc for a barrel surface) and rotation surfaces generated by a free-form curve.

Bridging this gap is, however, important when considering the several applications involving this typology of surfaces. Generic axial symmetric surfaces play a functional role, for example, in torque converters, in turbine and compressor casings and in the design of aerodynamic shapes. Recently, a profile of revolution of free form type has been suggested to optimize suitably the combustion chamber shape of a dual fuel engine [11]. Another example of application of generic axially symmetric surfaces can be found in the barrel-shaped rolling elements for radial bearings. The growing popularity of the additive manufacturing, finally, has been expanding the potential in the design of complex-shaped parts so that the application fields of the generic axially symmetric surfaces are expected to increase considerably in the near future.

Various approaches have been proposed for axis computation from triangularized models of generic axially symmetric surfaces. This paper first provides an overview of the approaches that can be used for geometric inspection purposes; then, it applies them to various case studies involving one or more generic axially symmetric surfaces, functionally important and for which the axis is to be detected since necessary for geometric inspection. The aim is to compare, therefore, the performances of the various methodologies by trying to highlight the circumstances in which these ones may fail. Since this investigation requires a

reference (i.e. the knowledge of the true axis), the methodologies have been applied to discrete models suitably extracted from CAD surfaces.
The choice to deepen this topic is partly due to the impact it has on the geometric verification of the product (especially with a view to automatic inspection) and partly due to the need of filling some gaps of ISO-GPS standards, whose standardization framework has remarkably been changing in these last years.
The paper is organized as follows. Section 2 describes the various approaches proposed in the literature highlighting, for each of them, the most significative implementations. Different estimates of the axis can be obtained according to the basic principle of the approach used and the particular implementation of the methodology under examination. Section 3 deals with some specific aspects relating to the implementation of the various methodologies and describes the case studies designed for this investigation. Section 4 discusses the results of the experimentation in order to draw useful information on how to choose the method and on the possible failure causes and modes. Finally, the conclusions are provided in section 5.

2. METHODOLOGIES FOR AXIS DETECTION

The approaches proposed to detect the axis from generic axially symmetric surfaces are various and differ in the specific property of these surfaces that has been considered. Following, these approaches have been described and classified based on these properties. Various methodologies can derive, obviously, from different implementations of a given geometric property.
Supposed that the axis of symmetry L is determined by a point $\boldsymbol{p_0}$ and a direction versor $\boldsymbol{v}$, the normals-based approach implements the property that the normal versor $\boldsymbol{n_i}$ at any point $\boldsymbol{p_i}$ of the surface always intersects the axis of symmetry (figure 1). As a result, the axis can be evaluated as the straight line that minimizes the sum of the squared distances of the normals from it. This approach estimates directly the axis from a single data input, consisting in the map of the normal versors $\boldsymbol{n_i}$ at each point $\boldsymbol{p_i}$ of the surface.

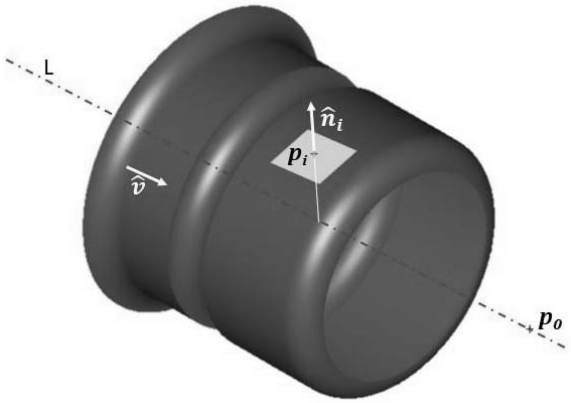

Figure 1. The property, which the normal-based approach is founded on.

Pottmann proposed a first implementation of this approach in [12]: it uses the normalized Plücker coordinates to represent a line. Based on this representation, the Plücker coordinates of the axis L, in figure 1, may be taken as $(\boldsymbol{v};\ \boldsymbol{v} \times \boldsymbol{p_0})$, where the vector product identifies the moment vector $\boldsymbol{m}$ of L with respect to the origin. If the moment vector is 0, the axis contains the origin of the Cartesian reference.
Given two generic lines respectively of moment vectors $\boldsymbol{m_1}$ and $\boldsymbol{m_2}$ and direction versors $\boldsymbol{v_1}$ and $\boldsymbol{v_2}$, the minimum distance *d* between them is given by the following formula:

$$d = \frac{|\boldsymbol{m_1} \cdot \boldsymbol{v_2} + \boldsymbol{m_2} \cdot \boldsymbol{v_1}|}{\|\boldsymbol{v_1} \times \boldsymbol{v_2}\|} \qquad (1)$$

If these two lines are incident, it follows that:

$$\boldsymbol{m_1} \cdot \boldsymbol{l_2} + \boldsymbol{m_2} \cdot \boldsymbol{l_1} = 0 \quad (2)$$

Since the normals at the points $\boldsymbol{p_i}$ of an axially symmetric surface intersect the axis of symmetry L, they satisfy, therefore, the following linear equations:

$$\boldsymbol{m_i} \cdot \boldsymbol{v} + \boldsymbol{m} \cdot \boldsymbol{n_i} = 0 \qquad (3)$$

where $(\boldsymbol{v};\boldsymbol{m})$ and $(\boldsymbol{n_i};\ \boldsymbol{m_i})$ are respectively the Plücker coordinates of the axis L and of the generic normal $\boldsymbol{n_i}$. In that condition, the set of normals at the points of a generic axially-symmetric surface is referred to as a singular linear complex.

For high-density discrete models acquired from real objects, the measurement noise and the surface irregularities (such as roughness and form errors) affect the estimation of the surface normals so that they cannot all intersect exactly the same straight line. In this case, the equation (3) is not rigorously verified and it can be rewritten by introducing the residual error $O(L,\boldsymbol{n_i})$:

$$\boldsymbol{m_i}\cdot\boldsymbol{v}+\boldsymbol{m}\cdot\boldsymbol{n_i}=O(L,\boldsymbol{n_i}) \qquad (4)$$

The set of Eq. (4) identifies a linear system of equations, where the Plücker coordinates of the axis L are the unknowns that have to verify the following two further conditions: $\|\boldsymbol{v}\|=1$ and $\boldsymbol{m}\cdot\boldsymbol{v}=0$.

The system can be solved by the least-squares method, which finds its optimum by minimizing the sum of squared residuals $O(L,\boldsymbol{n_i})$. Minimizing this sum, that is a positive semidefinite quadratic form, is then reduced to a generalized eigenvalue problem.

To cut down the influence of the outliers on the axis of symmetry so estimated, Halir proposed an additional step, based on the M-estimators, consisting in an iterative process aimed at the minimization of the sum S of weighted squared residuals $O(L,\boldsymbol{n_i})$ [13]:

$$S=\sum_i \omega_i O(L,\boldsymbol{n_i})^2 \qquad (5)$$

where the weights ω_i are evaluated, at each iteration of the method, by the Tukey's bi-weight function [14].

Another property of the axially symmetric surfaces used for axis estimation is that the center C_i of the sphere of curvature, tangent to the surface at the generic point $\boldsymbol{p_i}$ and intercepting the surface along the parallel passing through $\boldsymbol{p_i}$ and with constant principal curvature k_{p_i}, is located on the axis of the axially symmetrical surface (figure 2).

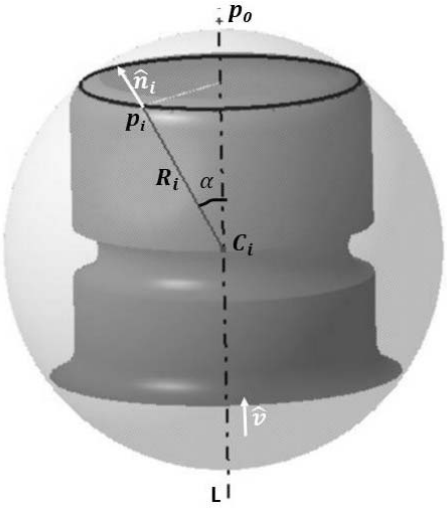

Figure 2. The property which the centers-based approach is founded on.

Several implementations of this approach, referred to as *centers-based approach*, have been proposed in the literature that differ from each other in the strategy used to find the axis. This strategy generally involves either the Hough transform or an optimization process.

The Hough transform is a robust and efficient tool for extracting geometric features [15-16]. It is based on a voting principle, according to which each geometric primitive will vote for the set of features, which it could belong to. This voting procedure is performed in a parametric space, from which object candidates are obtained as local maxima in a so-called accumulator space, which is explicitly constructed by the algorithm for the Hough transform computation. In [17] the authors estimated the rotational axis by applying the Hough transform to 2D projected images of centers of curvatures C_i. Sablatning and Menard proposed a similar approach in [18]. Under the hypothesis of surfaces with relatively small curvatures, the authors developed a method for the robust determination of the surface normals. These normals are then clustered in a 3D Hough-space and the axis of symmetry is estimated, directly, by fitting a line.

The major drawback of the methods for axis detection implementing the 3D Hough transform is that this tool becomes impractical, in terms of time and complexity, for analyses performed on high-density point clouds [19], such as those usually acquired by 3D laser scanners.

Among the methods that implement the centers-based approach with an optimization strategy, Mumford et al. proposed one of the most significant [20]. In this method, the 6-degrees of freedom necessary for axis identification are reduced to 4 by requiring that the point $\boldsymbol{p_0}$ on the axis is selected so that its distance from the origin is the minimum possible (i.e. the additional condition $\boldsymbol{p_0} \cdot \boldsymbol{v} = 0$ is imposed) and that $\|\boldsymbol{v}\| = 1$. The center of *sphere of curvature* at the point $\boldsymbol{p_i}$ is then identified by the following equation:

$$\boldsymbol{C_i} = \boldsymbol{p_i} - R_i \boldsymbol{n_i} = \boldsymbol{p_i} - \frac{\|(\boldsymbol{p_i} - \boldsymbol{p_0}) \times \boldsymbol{v}\|}{\|\boldsymbol{n_i} \times \boldsymbol{v}\|} \boldsymbol{n_i} \quad (6)$$

where R_i is the radius of the sphere, which is related to the curvature k_{p_i} of the surface parallel passing through $\boldsymbol{p}_i$, by the following relationship:

$$R_i = \frac{1}{k_{p_i} sin\, \alpha} \quad (7)$$

In (7), α is the angle identified by the normal versor $\boldsymbol{n_i}$ and the direction versor $\boldsymbol{v}$ of the axis L.
The axis estimation is then obtained by finding the line minimizing the sum of the least-squares distances from the estimated centers to it expressed by the following function:

$$F(\boldsymbol{p_0}, \boldsymbol{v}) = \sum_i \|(\boldsymbol{C_i} - \boldsymbol{p_0}) \times \boldsymbol{v}\|^2 \quad (8)$$

To retrieve an axis estimation, which was robust even with noisy data, weighted least-squares distances have been also implemented. Since (8) is nonlinear, its minimization requires a good initialization. In [20] Cao and Mumford used as initial estimate the axis obtained through the Pottmann et al.'s methodology [12].
The *symmetry lines-based* approach exploits the property whereby the symmetry line of any transverse section curve of an axially symmetric surface with complete angular spanning (or of a portion thereof in the case of incomplete spanning) always intersects the axis (figure 3).

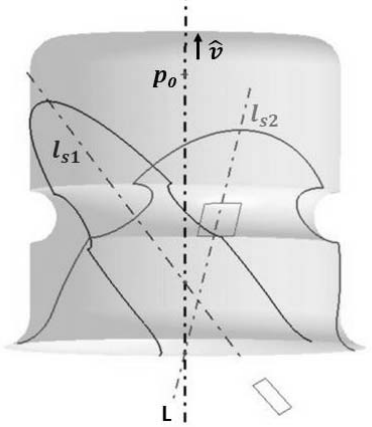

Figure 3. The property considered by the *symmetry lines-based approach.*

An implementation of this approach has been recently proposed in [21]. Figure 4 shows the flowchart of the various steps involved by this methodology. Firstly, the axially symmetric surface, given in the form of a tessellated model, is sliced by a set of transverse planes randomly identified. The generic resulting section curve is a polygon, whose vertices are generated by the intersection of the edges of the triangular facets with the section plane. These points are, then, sequentially connected to construct a polygonal curve.
The step of the symmetry line identification for the i-th transverse section, in the flow-chart of figure 4, is strategic because the quality of this phase of the implementation affects the accuracy of the method as a whole. A planar curve is reflection symmetric with respect to the line l_s if it is divisible into two mirror halves-located on both sides of the symmetry line l_s. This property is also satisfied in incomplete axially symmetric surfaces; but in such a case, the reflection symmetry is verified just for a portion of the curve. As stated before, in the case of a triangulated axially symmetric surface, the generic section profile is a polygonal curve and for this kind of curve, unfortunately, the property of reflection symmetry is never rigorously satisfied, mainly due to two reasons. Firstly, the vertices of the polygonal curve, both by position and by number, are not bilaterally symmetric with respect to the symmetry line. Secondly, the section curves, resulting from noisy discrete models extracted by real objects, are usually characterized by asymmetric geometric imperfections, such as cracks and dents.
As shown in the flow-chart of figure 4, the search for the symmetry line l_s is performed by an algorithm characterized by two main phases: curve mirroring and registration. In the first phase, a new curve is

generated by mirroring the original section curve. Then the mirrored curve is registered with respect of the original curve so that the best superimposition of both curves is obtained. This second phase implements the Iterative Closest Point (ICP) algorithm, which minimizes the squared distances between the vertices of the polygonal curve and those of its mirroring by means of the Levenberg-Maquardt algorithm. Once the registration process is complete, the symmetry line l_s is evaluated as the axis of the segment connecting the points of a curve to the corresponding ones of the mirrored registered curve. In order to enhance the convergence of the registration process, a preliminary estimation of the mirrored curve is obtained by mirroring the original section curve with respect to a line identified by one of its principal inertia components [21].

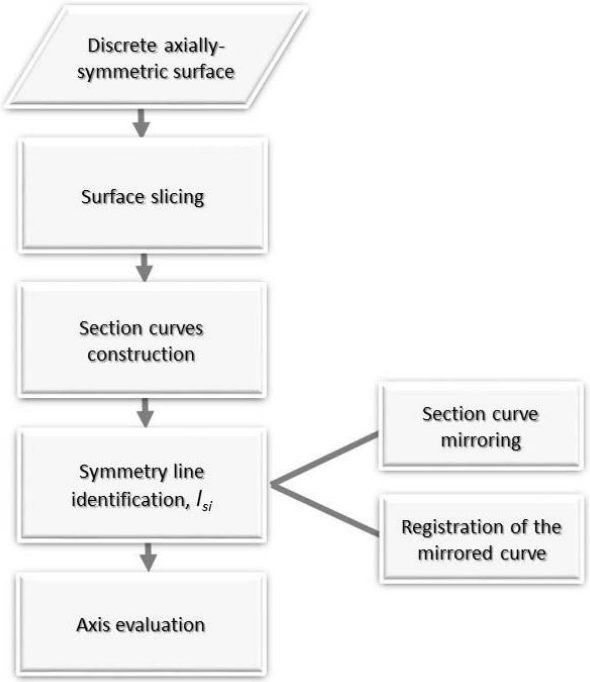

Figure 4. Flow-chart of the methodology implemented in [21] and based on the symmetry lines-based approach.

In some cases, however, the typical mirroring and registration algorithm can fail or give inaccurate results due to:

-local asymmetries;

-section curves that are only partially axially symmetric (since deriving from axially symmetric surface with incomplete circular spanning);

-location of vertices in the two symmetric halves that can differ a great deal owing both to differences in the surface sampling and to the measured surface imperfections.

In order to improve the accuracy of the mirroring and registration step, an enhanced version of the ICP algorithm was furtherly proposed [21]. This algorithm, in particular, aims at minimizing a new objective function, where the distance between the vertices of the two curves (original and mirrored) is replaced with the distance between the vertex of a curve and the nearest edge of the other. This allows also making the methodology insensitive to the asymmetries in vertices location.

The axis evaluation is performed, finally, implementing also in this case the normalized Plücker coordinates and therefore processing the set of symmetry lines as a singular linear complex. The first axis estimation is then refined by using the M-estimators, where the distances between the lines l_s and the axis L are minimized by using a weighted least-squares optimization, which gives more evidence to the symmetry lines characterized by low-values of registration errors.

Yet another approach for the axis computation implements the principal component analysis (PCA). This approach is based on the property that the axis of symmetry of a generic axially symmetric surface is one of the principal axes of inertia of the surface, whose points have got a mass conferred proportionally with the

area of the surface associated to the point. In the method proposed by Lao et al. [22], the axis is evaluated as one of the principal axes of inertia of the unit-mass point set of the Gaussian Map of the tessellated surface. To generate the Gaussian Map, the normal at the triangular facet is used, whose length is proportional to the facet area. This method is obviously suitable only for processing complete spanned surfaces.

Finally, there is the approach referred to as "circle and line fitting" methodology. This approach takes advantage of the property whereby each section perpendicular to the axis of a generic axially symmetric surface is a circle, whose center c_i lies on the axis (figure 5). Based on this property, first, the ideal circular features to associate with the non-ideal integral circles (extracted by the transverse cutting of the surface through a suitable bundle of parallel planes) are identified. Then the axis is estimated as the least-squares line approximating the centers c_i of these ideal circles.

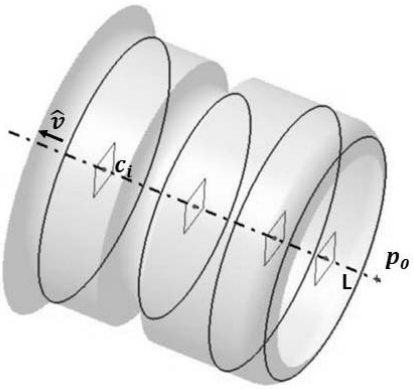

Figure 5. Working principle of the "circle and line fitting" approach.

An iterative process has been proposed for obtaining a more refined axis estimate in which the axis is identified, at each iteration, from a bundle of planes that is perpendicular to the axis direction estimated from the previous iteration [13].

3. METHODS IMPLEMENTATION AND CASE STUDIES

The methodologies just described can be classified into direct or indirect. The direct approaches are able to evaluate directly the axis without requiring any preliminary estimation. It is worth noting that the axis evaluated with a direct methodology (such as the normal–based methodology) is often refined by a following optimization step (e.g. the M-estimators) which, through an iterative process, aims at converging towards a better estimate. This makes the implementation of the approach more powerful overall and with the only drawback of an increased computational cost.

Table 1. Classification of the approaches into direct and non-direct

Methodology	*Direct*	*Non-direct*
Normal–based	x	-
Centers-based	-	x
Symmetry lines-based	x	-
PCA approach	x	-
Circle and line fitting	-	x

Although the centers-based approach does not need any first-attempt axis, this estimate may come in handy to establish which of the principal directions has to be used for the identification of the centers of curvature considered by the method. A preliminary estimate of the axis is necessary, on the other hand, in the

implementation of this approach proposed by Mumford et al. in [20], because the algorithm is based on an optimization process that iteratively searches for the best solution.
In the circle and line fitting method, the preliminary axis is an important input in order to construct the first bundle of planes (perpendicular to it) by which to extract the non-ideal integral circles from the surface. The quality of this first-attempt estimate affects significantly the accuracy of the final axis evaluation. In [13], for example, the preliminary axis is obtained by the normal-based methodology proposed in [12] and then refined by the M-estimators.
Table 2 shows the methodologies that have been chosen to implement for each approach, together with the references to the papers detailing them.

Table 2. The set of the methodologies selected here for the implementation.

Approach type	*Methodology implemented*
Normal–based approach	• Pottmann implementation (referred to as *P-*) [12]. • P-methodology refined with M-estimators (referred to as *M_e-*) [13].
Centers-based approach	Mumford implementation (referred to as *Mu-*) [20].
Symmetry lines-based approach	Transverse sectioning methodology (referred to as *Sect-*) [21]
PCA approach	Lao implementation (referred to as *Lao-*) [22]
Circle and line fitting approach	Halir implementation [13] (referred to as *Hal-*).

All the methodologies of table 2 have been implemented here in an original software package coded in MATLAB that takes in the .stl file of the tessellated axially symmetric surface and outputs the various axis estimates.
The methodologies that implement the normal–based approach need, obviously, an accurate and robust estimation of the normals at the mesh nodes. Since this evaluation can affect significantly the axis estimate, in this paper the vertex normals are computed according to the medial quadric approach [23]: this is a discrete method whose main advantage is to be independent from triangles shape and dimensions.
For the methodologies that require it, the axis estimate according to the P-methodology has always been used as first-attempt axis.
As regards the Hal-methodology, the authors propose to add here a further step to the implementation described in [13] in order to minimize the influence of the outliers on the axis final estimate. At the end of the kth-iteration, the distances d_j between the axis $\bar{l}_k$ just estimated and the center c_j of the jth ideal circle, identified by the methodology proposed in [24], are computed for all the centers. In agreement with the *Tukey's bi-weight* formulation, if the following inequality:

$$d_j \geq \sigma\, c \quad (9)$$

with $\sigma = 1.4826 \underset{j}{median}(d_j)$ and $c = 4.6851$, is verified then the distance d_j is excluded from the objective function for the axis least-squares evaluation, that will be minimized at the next iteration.
As far as the implementation of the other methodologies is concerned, no further details are required except that of referring to the related papers shown in table 2.
The experimentation has been carried out on several discrete geometric models suitably extracted by CAD descriptions of generic axisymmetric surfaces.
Each case study includes one or more generic axial symmetric surfaces that are functionally important and for which a robust axis identification is a key pre-requisite for verifying suitably the product conformance during the geometric inspection. In most cases, these surfaces have characteristics (in terms of geometry, resolution, and regularity of the mesh) that are critical to the methodologies for the axis evaluation.
The first case study, shown in fig. 6 and referred here to as TC#1, is a slightly barrel-shaped symmetrical roller of a CARB toroidal roller bearing, designated as C 39/630 M according to IS0 15 [25]. This category of bearing accommodates exclusively radial loads and it is largely used as non-locating bearing in large electric motors, due to its capability to perform well both with low and large loads. The tolerance values for this type of radial roller bearing are established by ISO 492 [26].

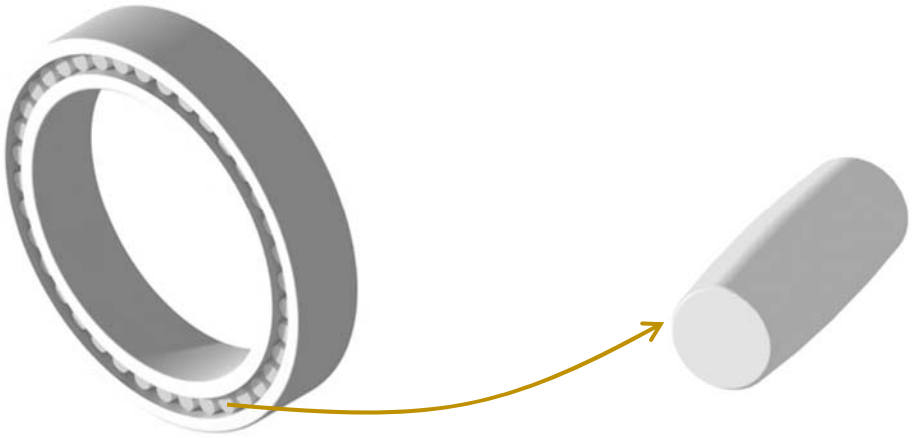

Figure 6. The case study TC#1: a barrel-shaped symmetrical roller from a C 39/630 M bearing.

The case study TC#2 is a 29-inch wheel for a bike (Figure 7 a), for which two generic axial symmetric surfaces, functionally important and not referable to cones and cylinders, can be identified. Figure 7 b shows the longitudinal profile of the two surfaces, that is a free-form curve in both cases. The conformity of these surfaces to the ISO specifications, whose verification involves the axis estimation, is essential to guarantee the proper dynamical behaviour of the bike. The axis identification from these surfaces, however, is expected to be challenging since they are characterized by a low value of the ratio τ between the height l (measured along the axis of revolution) and the maximum transverse radius (R_{max}).

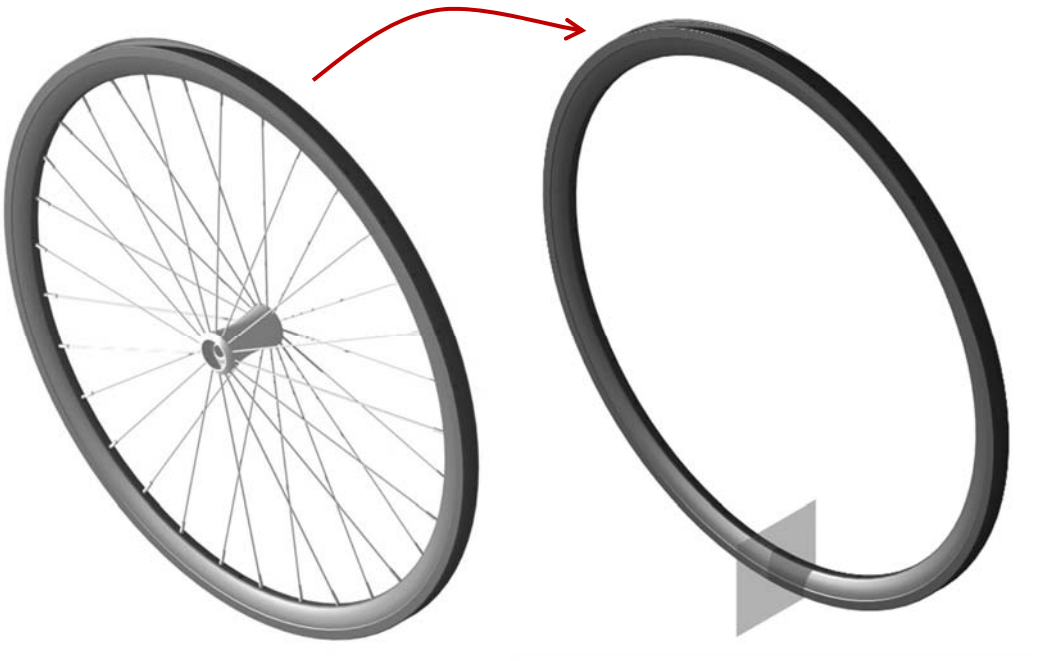

a)

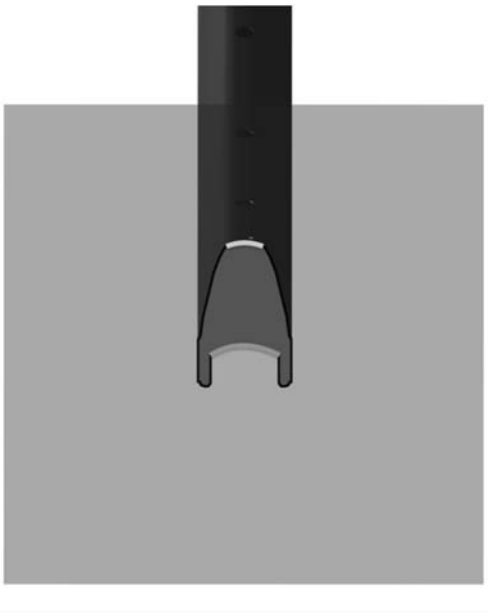

b)

Figure 7. The 29-inch wheel considered for the case study TC#2 (a); the longitudinal prof the two surfaces considered for experimentation (b).

The last case study TC#3 is one of the three radial components that make up the lip skin linking the internal and external fan cowls of a turbofan engine. In particular, the lip skin of an Airbus 32x family aircraft, powered by a CFM 56 turbofan engine, has been taken as reference. The nominal surface of this component is generated by the axial revolution with incomplete angular spanning of a free-form profile, whose shape is functionally important for fluid-dynamic reasons. Since it is a very large component (the R_{max} value is approximately equal to 2.5 meters), even a slight deviation from the nominal axis can lead to assembly problems with the other components of the lip skin.

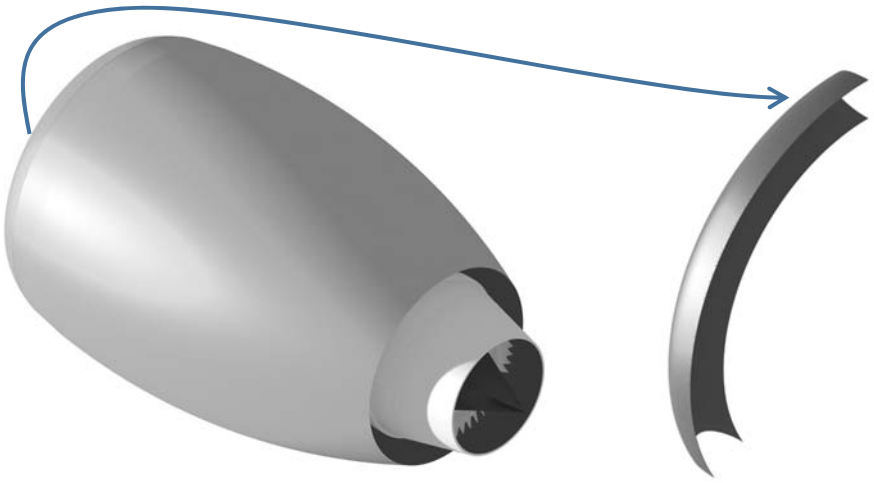

Figure 8. The case study TC#3: one of the radial components of the lip skin from a CFM 56 turbofan engine.

For each case study, a discrete geometric model has been synthetically obtained by the tessellation of the CAD surface with a random distribution of nodes. This type of tessellation made it possible to generate mesh whose nodes, are not located perfectly on the transition between the faces of the CAD model (i.e. on sharp or tangent edges). So doing, it is possible to obtain discrete models well simulating those generated by the 3D scanning of real objects.

In the perspective of a geometric verification process, the partition of the discrete model into a set of non-ideal features is a crucial step since the characteristics to verify during the geometric inspection have to be extracted or derived by the features which a GPS specification is applied to. In this paper, the characteristics are the axes of the surfaces pointed out in the figures 9, 10 and 11 for the case studies respectively TC#1, TC#2 and TC#3. To extract the related non-ideal features, the discrete model has been automatically partitioned here by applying the methodology for feature segmentation proposed in [27]. Secondary features, such as the fillets and rounds in TC#1 and TC#2, have been also automatically detected and removed implementing the approach described in [5, 6].
To take into account the effect of measurement noise and surface irregularities (such as roughness and form errors) on high-density models experimentally acquired from real objects, the Gaussian noise has been added to the discrete models to be investigated. It has been hypothesized, in particular, that due to the effect of the applied noise, the vertices of the mesh move along the corresponding vertex normals calculated for the unnoisy model with the methodology proposed in [23]. In particular, for each non-ideal feature, from which deriving the axis through the methodologies considered here, three increasing levels of noise have been added and, for each of them, 5 noisy discrete models generated. The levels of noise are Σ, 5Σ and 10Σ, where Σ, the standard deviation, is equal to 0.01, 0.007 and 0.1 respectively for TC#1, TC#2 and TC#3.

4. RESULTS

All the results of the experimentation are collected in the tables of the figures 9, 10 and 11.
Since the true axis of each non-ideal feature to investigate is known and coincident with the axis of the related CAD model, the errors in the axis estimates are evaluated in terms of angular and distance deviations from the true axis. For this reason, the results have been organized here into two tables: the left one is for angular deviations, the right for distance deviations (i.e. the minimum distance between the ideal and the estimated axis).
For each surface to investigate, the angular spanning (span), the bounding box dimensions (l, w and h) and the values for R_{max} and τ are reported. The average edge length (d_{mean}) with the related standard deviation (σ_d) are also shown for the various non-ideal features to investigate.
In both the tables of results, the first column lists the values of the two deviations in the ideal (i.e. unnoisy) case. The other columns show the mean errors on 5 axis estimates obtained with a specific methodology for the levels of noise Σ, 5Σ and 10Σ.

TC#1$_{sup1}$

span	360 deg
l	125.48 mm
w	48.81 mm
h	48.81 mm
R_{max}	24.41
τ	5.14

TC#1$_{sup1}$

mesh properties	
σ_d	*d_{mean}*
0.09	0.92

angle [deg]	*no noise*	*Σ*	*5Σ*	*10Σ*
P	0.00	0.00	0.00	0.01
M_e	0.00	0.00	0.00	0.01
Mu	0.00	0.00	0.00	0.00
Hal	0.00	0.08	0.01	0.00
Sect	0.00	0.00	0.01	0.01
Lao	0.01	0.01	0.01	0.01

distance [mm]	*no noise*	*Σ*	*5Σ*	*10Σ*
P	0.00	0.00	0.01	0.01
M_e	0.00	0.00	0.01	0.01
Mu	0.00	0.00	0.00	0.00
Hal	0.00	0.03	0.02	0.01
Sect	0.00	0.00	0.00	0.01
Lao	0.01	0.01	0.02	0.01

Figure 9. The results of the experimentation for TC#1 (Σ = 0.01).

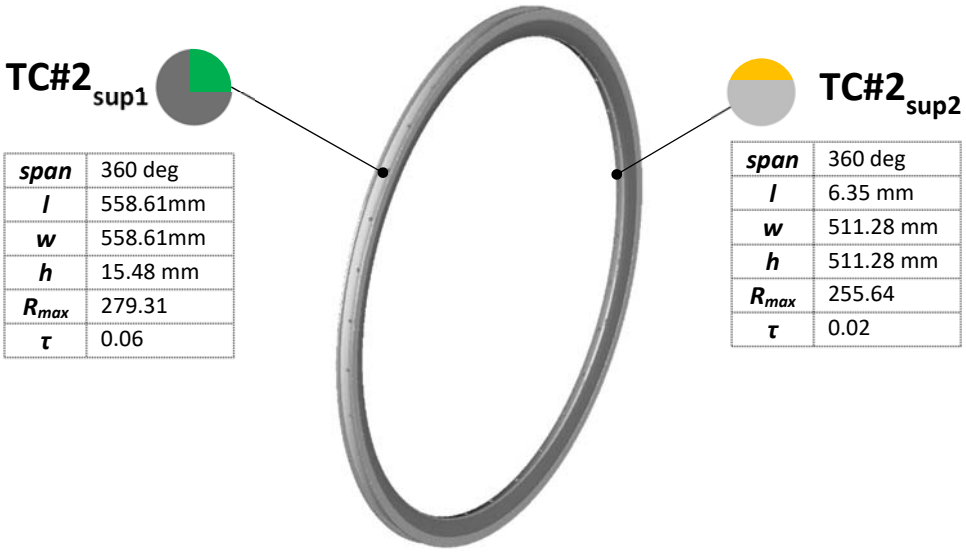

TC#2$_{sup1}$

span	360 deg
l	558.61mm
w	558.61mm
h	15.48 mm
R_{max}	279.31
τ	0.06

TC#2$_{sup2}$

span	360 deg
l	6.35 mm
w	511.28 mm
h	511.28 mm
R_{max}	255.64
τ	0.02

TC#2$_{sup1}$

mesh properties	
σ_d	d_{mean}
0.07	0.54

angle [deg]	*no noise*	*Σ noise*	*5Σ noise*	*10Σ noise*
P	0.00	0.00	0.01	0.03
M_e	0.00	0.00	0.01	0.03
Mu	0.00	0.01	0.01	0.05
Hal	0.00	0.00	0.00	0.01
Sect	0.06	0.13	0.21	--
Lao	0.04	0.04	0.03	0.03

distance [mm]	*no noise*	*Σ noise*	*5Σ noise*	*10Σ noise*
P	0.06	0.05	0.06	0.02
M_e	0.05	0.06	0.05	0.10
Mu	0.06	0.05	0.05	0.06
Hal	0.14	0.11	0.83	3.23
Sect	3.01	3.01	3.01	--
Lao	1.07	1.06	1.05	1.03

TC#2$_{sup2}$ (M_1)

mesh properties	
σ_d	d_{mean}
0.35	0.70

angle [deg]	*no noise*	*Σ noise*	*5Σ noise*	*10Σ noise*
P	0.05	0.05	0.12	36.26
M_e	0.05	0.05	0.12	1.69
Mu	90.00	89.99	89.91	89.99
Hal	0.05	0.04	0.13	36.26
Sect	89.90	89.86	0.95	6.41
Lao	0.07	0.07	0.11	0.06

distance [mm]	*no noise*	*Σ noise*	*5Σ noise*	*10Σ noise*
P	0.01	0.13	0.31	13.91
M_e	0.01	0.16	0.32	0.37
Mu	5.4E+4	3.9E+4	3.8E+3	2.6E+4
Hal	0.10	8.24	3.15	13.91
Sect	6.0E+4	8.2E+4	0.05	0.52
Lao	7.00	7.00	7.02	6.97

TC#2$_{sup2}$ (M_2)

mesh properties	
σ_d	d_{mean}
0.21	0.68

angle [deg]	*no noise*	*Σ noise*	*5Σ noise*	*10Σ noise*
P	0.01	0.02	0.20	1.72
M_e	0.01	0.02	0.20	1.37
Mu	0.01	0.02	0.21	0.68
Hal	0.00	0.00	0.07	0.71
Sect	0.28	2.30	4.04	5.52
Lao	0.11	0.11	0.11	0.14

distance [mm]	no noise	Σ noise	5Σ noise	10Σ noise
P	0.01	0.19	0.22	0.17
M_e	0.01	0.19	0.33	0.80
Mu	0.06	0.19	0.24	0.20
Hal	0.04	21.88	19.87	13.75
Sect	3.01	1.53	2.70	3.63
Lao	1.07	1.37	1.34	1.26

TC#2$_{sup2}$ (M_3)

mesh properties	
σ_d	d_{mean}
0.27	0.86

angle [deg]	*no noise*	*Σ noise*	*5Σ noise*	*10Σ noise*
P	0.01	0.11	0.77	0.24
M_e	0.02	0.10	0.54	0.23
Mu	0.01	0.18	0.14	0.05
Hal	0.00	0.04	0.02	0.14
Sect	1.06	2.52	5.88	5.52
Lao	0.14	0.13	0.19	0.17

distance [mm]	*no noise*	*Σ noise*	*5Σ noise*	*10Σ noise*
P	0.02	0.12	0.08	0.22
M_e	0.02	0.33	0.14	0.21
Mu	0.01	0.11	0.03	0.17
Hal	0.02	9.03	0.13	0.24
Sect	0.70	1.69	3.83	3.61
Lao	1.29	1.38	1.18	1.36

Figure 10. The results of the experimentation for TC#2 (Σ = 0.007).

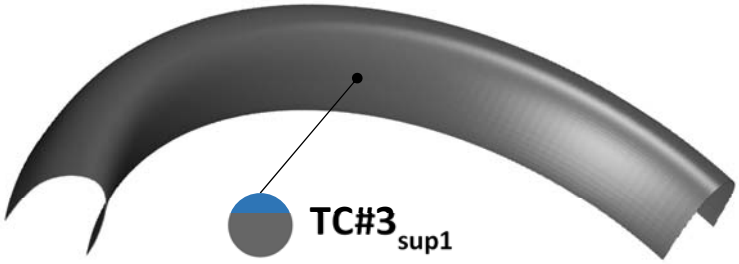

span	120 deg
l	502.44 mm
w	2550 mm
h	3824.97 mm
R_{max}	2550 mm
τ	0.1

TC#3$_{sup1}$

mesh properties	
σ_d	d_{mean}
0.53	3.78

angle [deg]	*no noise*	*Σ*	*5Σ*	*10Σ*
P	0.00	0.02	0.43	89.98
M_e	0.00	0.02	0.42	89.98
Mu	90.00	90.00	90.00	90.00
Hal	0.00	0.02	0.40	89.98
Sect	--	--	-	-
Lao	44.12	1.65	1.51	1.04

distance [mm]	*no noise*	*Σ*	*5Σ*	*10Σ*
P	0.00	1.32	28.16	1000.28
M_e	0.00	1.31	26.23	1184.41
Mu	985.73	985.72	985.72	1003.50
Hal	0.00	1.30	27.27	1263.77
Sect	--	--	-	--
Lao	981.82	981.82	981.88	981.74

Figure 11. The results of the experimentation for TC#3 (Σ = 0.1).

The deviations for TC#1$_{sup1}$ (figure 9) show that the errors are negligible for all the methods considered here. This result was actually expected, as TC#1$_{sup1}$ is with complete angular spanning and has a rather high τ-value (slightly higher than 5). A previous investigation, although limited to only three methodologies among those considered here, pointed out this result in the case of cylindrical or conical surfaces extracted from real mechanical components [28]. A slight instability of the Hal-methodology, which should ideally refine the axis estimate according to the P-methodology, is also detectable for TC#1$_{sup1}$ in the presence of noise.

The case study TC#2, although including two surfaces with a still complete angular spanning, is potentially more critical than TC#1. The surfaces are characterized by a ratio τ of two orders of magnitude lower than the value of TC#1 (0.06 and 0.03 respectively for TC#2$_{sup1}$ and TC#2$_{sup2}$). For such low τ-values, the axis estimate is expected to become more sensitive to the resolution and regularity of the mesh as well as to the level of Gaussian noise added.

In the specific case of TC#2$_{sup1}$, the deviations (in terms of distance especially) with the Lao- and Sect-methods increase significantly compared to the errors obtained for TC#1 with the same methodologies. The Sect-method, additionally, fails to converge when the highest noise level is added. For the other methodologies, the distance deviations are slightly higher than those ones for TC#1 even in the absence of noise. Among these, however, the estimates obtained with the Hal-methodology are of an order of magnitude higher and degenerate faster as the noise level increases.

For TC#2$_{sup2}$, three different samplings of the CAD model (referred respectively to as M_1, M_2 and M_3 in the corresponding boxes of the figure 10) have been carried out in order to investigate the methodologies behaviour for different values of resolution (d_{mean}) and regularity of the mesh (σ_d). Particularly, M_1 and M_2 differ for regularity, while M_2 and M_3 for resolution. The tessellations M_1, M_2 and M_3 are, additionally, more critical than TC#2$_{sup1}$ in terms of resolution and regularity, and the surface TC#2$_{sup2}$ is characterized by the lowest τ-value.

The poor estimates obtained with the Sect and Lao-methods for M_1, M_2 and M_3 confirm the difficulty that these methodologies encounter in evaluating the axis of axisymmetric surfaces with τ-values highly lower than 1. Compared to what was found for TC#2$_{sup1}$, the axes estimates according to the Hal-methodology

worsen faster and less predictably as soon as noise is added. For most of the tests carried out, the Hal-method is not able to refine the first-attempt axes, although of good quality, showing a rather widespread and marked instability.

As for the other methodologies, the most evident result for M_1 is the failure of the Mu-methodology. The experimentation carried out on M_2 and M_3 confirmed that this is due to the poor regularity of M_1. A generalized improvement in the quality of all estimates is, actually, observed when the mesh regularity increases (with the same resolution), as well as a deterioration when the mesh resolution becomes poorer.

TC#3 is another case study critical for the methodologies considered here. TC#3_{sup1} is a generic axially symmetric surface coming from the incomplete revolution of a free form curve around the axis. Due to incomplete angular spanning, the Lao- method gives poor results as expected, while the Sect-method is able to provide no estimates, failing the symmetry lines identification from transverse profiles. The remaining methods, except for the Mu-methodology, provide axis estimates of good quality in the ideal case. As the noise increases, however, a generalized and very fast worsening of all the estimates is observed.

The Mu-methodology surprisingly fails for TC#3_{sup1} both in the absence and in the presence of noise. This behaviour, however, cannot be justified here with the sensitivity, previously highlighted, of the Mu-methodology to the regularity of the mesh, since the tessellation carried out for TC#3_{sup1} is of high quality.

A thorough investigation of the case study shows that this failure is due to an intrinsic limitation to the Mu-methodology and not to the incomplete angular spanning of the surface. The Mu-methodology, in fact, is sensitive to the sign of the direction of the vertex normal. The equation (6), which identifies the center of the sphere of curvature at the generic point $\boldsymbol{p_i}$ of the surface, holds for axially symmetric surfaces characterized by vertex normals whose direction points away from the axis, as happens for example for the outer surface of a cylindrical tube. To extend the applicability of this equation, a modification to the Mu-methodology has been proposed in [29]. This modification involves computing the function (8) twice, first with the original direction of the normal versors and then with their reverse. The final estimate for the axis is, therefore, that for which the function (8) reaches the minimum value.

For TC#3_{sup1}, however, this trick cannot be used at all since it is not possible to identify a homogeneous orientation of the vertex normals: some normals, in fact, point towards the axis and others do not, as shown in Figure 12 for a set of randomly chosen points on the surface. Since the true axis of TC#3_{sup1} is known, it is possible to partition this surface into two regions with homogeneous orientation of the normals. Applying the Mu-methodology to each of them, axis estimates of good quality have been obtained. It is thus confirmed that it is the particular shape of the longitudinal profile and not the angular incompleteness of the surface that explains the bad behaviour of the Mu-methodology when applied to the surface TC#3_{sup1} as a whole.

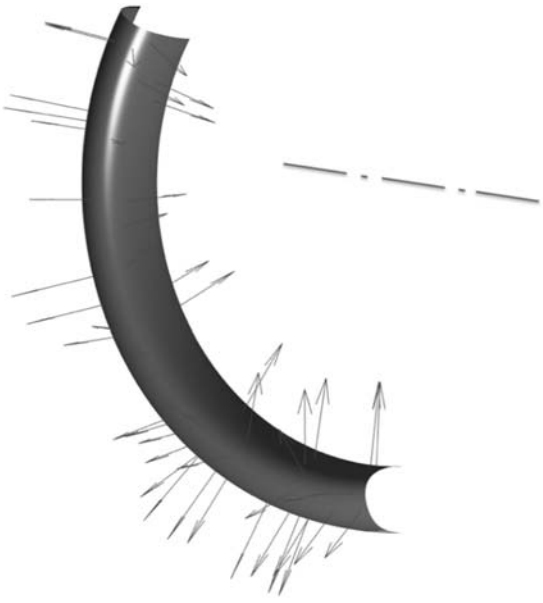

Figure 12. Vertex normals for a set of points chosen at random on TC#3sup1.

Actually, the shape of the longitudinal profile of TC#3$_{sup1}$ is potentially a problem also for the Hal-methodology, especially if the preliminary axis from which the method starts is not of good quality. For this specific case study, in fact, the transverse cutting of the surface through a bundle of planes perpendicular to the axis of revolution gives a couple of circular and concentric arcs for each plane (figure 13 a). For increasing angular deviations of the preliminary axis with respect to the true axis, on the other hand, the transversal profile is or a couple of non-circular arcs or a single curve of complex shape. Figure 13 b, for example, shows the sections obtained by cutting *TC#3$_{sup1}$* with planes perpendicular to a preliminary axis inclined of 0.6 deg with respect to the true axis. Some tests, in which several first-attempt axes with increasing angular deviations are given as inputs to the Hal-methodology, have been performed by confirming the rapid deterioration of the estimates in output.

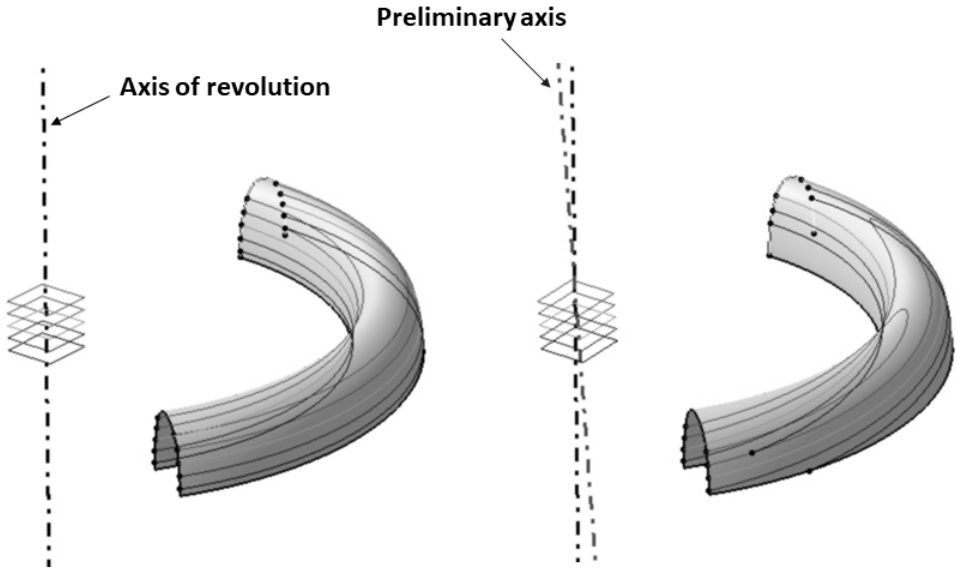

Figure 13. The transverse profiles obtained by cutting TC#3sup1 with a bundle of planes perpendicular to: (a) the axis of revolution; b) a preliminary axis inclined of 0.6 deg with respect to the true axis.

In conclusion, the experimentation shows that the normals-based methods are generally the most accurate and robust ones. Furthermore, not suffering from particular geometric limitations (such as, for example, the Hal- and Mu-methodologies for the surfaces characterized by a non-homogeneous orientation of the vertex normals) they are also very flexible. Preferring the M_e- to the P-methodology, however, does not seem generally justified, because the relative estimates of the axis, in most cases very close to each other, are computationally more onerous.

It is worth noting that the results of this investigation are valid for synthetic case studies affected, at most, by Gaussian noise. Very different results can be obtained if, for example, case studies with local defectiveness were considered. Actually, a study in this regard has already been proposed in [21], showing that the method for axis computation least affected by surface defects was the Sect-methodology.

In the Table 3, the main results of the analysis carried out here are reported, framing the limits of applicability of the various tested algorithms.

Table 3. Limits of applicability of the various tested algorithms.

Geometric features	- Complete span - $\tau > 1$	- Complete span - $\tau << 1$	- Incomplete span - $\tau << 1$	- Surface with non-homogeneous orientation of the normals
Well-working methods	✓ P ✓ M_e ✓ Mu ✓ Hal ✓ Sect ✓ Lao	✓ P ✓ M_e ✓ Mu	✓ P ✓ M_e ✓ Mu ✓ Hal	✓ P ✓ M_e ✓ Sect ✓ Lao
Failing methods		✗ Hal ✗ Sect ✗ Lao	✗ Sect ✗ Lao	✗ Mu ✗ Hal
Notes on well-working models	Hal-estimates are slightly instable for noisy models.	Mu needs regular tessellations.	The methods are highly sensitive to noise.	The P/M_e/Sect/Lao behaviour follows what has been reported in the other columns.

5. CONCLUSIONS

Metrological inspection often requires the evaluation of the axis in order to verify the conformity of the product to the GPS specifications necessary to control geometric properties of functional importance. The quality of the axis estimate can significantly influence the reliability of the geometric verification so that the accuracy of this evaluation is actually a critical factor to consider. Axis, however, is not an integral feature, therefore it has to be derived from the points extracted during the measurement of the related surface. This makes the axis detection a very complex task to accomplish.

The ISO standards address this issue only in the case of cylinders and cones. No information is provided, however, on how to carry out this estimate when the axially symmetric surface is of generic type. Bridging this gap, however, is important when considering the increasing number of mechanical applications where generic axially symmetric surfaces play a functional role.

This paper, which is focused on that objective, first provided an overview of the approaches in the literature that can be used in the perspective of a geometric product verification. Original implementations of several methodologies have been applied to a set of synthetic case studies, suitably designed in order to investigate the circumstances in which the various methodologies may fail. The behavior of these methodologies has been investigated in relation to various aspects related to surface geometry (i.e. ratio τ, angular spanning and longitudinal profile shape), mesh properties (i.e. regularity and density) and sensitivity to the noise. Particular attention has been paid to the identification of those situations that can be critical for an accurate and robust axis computation. Several useful information, finally, in terms of applicability of the algorithms as well as of the failure causes and modes have been provided.

REFERENCES

[1]. ISO 1101: 2017. Geometrical product specifications (GPS) — Geometrical tolerancing — Tolerances of form, orientation, location and run-out.

[2]. Di Angelo L, Di Stefano P and Morabito AE. The RGM data structure: a nominal interpretation of an acquired high point density model for automatic tolerance inspection, *International Journal of Production Research*, 2012, 50(12), 3416-3433.
[3]. Di Angelo L, Di Stefano P and Morabito AE. Automatic evaluation of form errors in high-density acquired surfaces, 2011, *International Journal of Production Research*, 49(7), 2061-2082.
[4]. Guardiani E and Morabito AE. Towards the Automation of Product Geometric Verification: An Overview. 2020, *Computer-Aided Design & Applications*, 17(5), 900-920.
[5]. Di Angelo L, Di Stefano P and Morabito AE. Fillets, rounds, grooves and sharp edges segmentation from 3D scanned surfaces, 2019, *Computer Aided Design*, 110, pp. 78-91.
[6]. Di Angelo L, Di Stefano P and Morabito AE. Secondary features segmentation from high-density tessellated surfaces, 2018, *International Journal on Interactive Design and Manufacturing*, 12 (3), pp. 801-809.
[7]. ISO 2768: 1989. General tolerances - Part 1: Tolerances for linear and angular dimensions without individual tolerance indications and Part 2: Geometrical tolerances for features without individual tolerance indications
[8]. ISO 17450-3:2016. Geometrical product specifications (GPS) – General concepts – part 3: Part 3: Toleranced features.
[9]. ISO 17450-1. 2011. Geometrical product specifications (GPS) – general concepts – part 1: model for geometric specification and verification.
[10]. ISO 22432:2011. Geometrical product specifications (GPS) — Features utilized in specification and verification.
[11]. Donateo T, Tornese F and Laforgia D. Computer-aided conversion of an engine from diesel to methane, 2013, *Applied Energy*, 108, pp. 8-23.
[12]. Pottmann H, Peternell M and Ravani B. An introduction to line geometry with applications. 1999, *Computer Aided Design*, 31:13–6.
[13]. Halir R. An automatic estimation of the axis of rotation of fragments of archaeological pottery: a multi-step model-based approach. In: *Proceedings of the seventh international conference in central Europe on computer graphics*. Visualization and interactive digital media (WSCG'99). 1999.
[14]. Barnett V and Lewis T. *Outliers in statistical data*. New York: John Wiley & Sons, 1984.
[15]. Hoffelder M, Sauer K and Rigby J: A Hough transform technique for detection of rotationally invariant surface features. In: *Proceedings of 1st international conference on image processin*g, pp. 944– 948. Austin, 1994, 9.
[16]. Yip PTRK, Lam WC and Leung D. A Hough transform technique for the detection of rotational symmetry. *Pattern Recognition Letters*, 1994, 15(9919), 919–928.
[17]. Yokoya N and Levine M. Volumetric shapes of solids of revolution from a single-view range image. *Computer vision, graphics and image processing: image understanding*, 1994, 59(1), 43–52.
[18]. Sablatnig R and Menard C. On estimating the position of fragments on rotational symmetric pottery. In: *Proceedings of the second international conference on 3-D imaging and modelling* (3DIM'99), 1999, Ottawa, pp. 455–462.
[19]. Rabbani T and van den Heuvel FA. Efficient Hough transform for automatic detection of cylinders in point clouds. In: *Proceedings of international archives of photogrammetry, remote sensing and spatial information sciences workshop*, 2005, Enschede, pp. 60–65.
[20]. Cao Y, Mumford D. Geometric structure estimation of axially symmetric pots from small fragments, *Signal Processing, Pattern Recognition, and Applications*, 2002, IASTED International Conference.
[21]. Di Angelo L, Di Stefano P and Morabito AE. A robust method for axis identification. 2015, *Precision Engineering*, 39, 194–203.
[22]. Lao YZ, Leong HW, Preparata FP and Singh G. Accurate cylindricity evaluation with axis-estimation preprocessing. 2003, *Precision Engineering* 27:429–37.
[23]. Jiao, X., Alexander P.J.: Parallel feature-preserving mesh smoothing. In: Proceedings of international conference on computational scienceanditsapplications2005,pp.1180–1189.Singapore(2005)
[24]. Taubin, G. Estimation of Planar Curves, Surfaces, and Nonplanar Space Curves Defined by Implicit Equations with Applications to Edge and Range Image Segmentation, (1991) IEEE Transactions on Pattern Analysis and Machine Intelligence, 13 (11), pp. 1115-1138.
[25]. ISO/CD 492 - Rolling bearings — Radial bearings — Geometrical product specifications (GPS) and tolerance values.
[26]. ISO 15:2017 - Rolling bearings — Radial bearings — Boundary dimensions, general plan.

[27]. Di Angelo L, Di Stefano P and Morabito AE. Recognition of intrinsic quality properties for automatic geometric inspection, International Journal on Interactive Design and Manufacturing, 2013, 7(4), 203-215.
[28]. Di Angelo L, Di Stefano P and Morabito AE. Comparison of methods for axis detection of high-density acquired axially-symmetric surfaces, *International Journal on Interactive Design and Manufacturing*, 2014, 8 (3), 199–200.
[29]. Hong, J.H., Kim, Y.M., Wi, K.-C., Kim, J. PotSAC: A robust axis estimator for axially symmetric pot fragments. (2019) Proceedings - 2019 International Conference on Computer Vision Workshop, ICCVW 2019, art. no. 9022556, pp. 1421-1428.